XII Simpósio Brasileiro de Automação Inteligente (SBAI)
Natal – RN, 25 a 28 de outubro de 2015

WHOLE-BODY MODELING AND CONTROL OF AN UNMANNED AERIAL MANIPULATOR

Laysa Santos Mello*, Bruno Vilhena Adorno*, Guilherme Vianna Raffo*

*Universidade Federal de Minas Gerais
Av. Antônio Carlos 6627, Belo Horizonte, MG 31270-010 Brasil

Emails: laysamello@ufmg.br, adorno@ufmg.br, raffo@ufmg.br

Abstract— This paper presents the whole-body modeling and control of a quadrotor unmanned aerial vehicle serially coupled to a three-link manipulator. Dual quaternion algebra is used to obtain the kinematic model, and the dynamic model expresses the influence of the manipulator movement in the center of mass of the entire system. The proposed control strategy uses a cascade layout comprising a kinematic controller and an inverse dynamics controller, whose main objective is to track a desired trajectory for the end-effector while keeping the system stable. Finally, the performance of the proposed control strategy is evaluated through simulation results, showing that a trajectory defined for the manipulator end-effector is successfully tracked while the quadrotor remains stable.

Keywords— Unmanned Aerial Vehicle, Dual Quaternions, Whole-Body Modeling, Underactuated System Control.

Resumo— Este trabalho apresenta a modelagem de corpo completo e controle de um veículo aéreo não tripulado tipo quadrirrotor acoplado a um manipulador de três elos. A modelagem cinemática utiliza a álgebra de quatérnios duais e o modelo dinâmico expressa a influência do movimento do manipulador no centro da massa de todo o sistema. A estratégia de controle proposta utiliza um *layout* em cascata, composto por um controlador cinemático e um controlador de dinâmica inversa, sendo seu principal objetivo acompanhar a trajetória desejada para o efetuador enquanto mantém o sistema estável. Finalmente, o desempenho da estratégia de controle proposta é avaliado através de resultados de simulação, mostrando que uma trajetória definida para o efetuador do manipulador é rastreada com sucesso enquanto o quadrirrotor se mantém estável.

Palavras-chave— Veículos Aérios não Tripulados, Quatérnios Duais, Modelagem de Corpo Completo, Controle de Sistema Subatuado.

1 Introduction

Mobile manipulators have attracted much attention in academic research in recent years, thanks to the mobility offered by the mobile platform and the manipulation capabilities offered by the manipulator (Adorno, 2011; Jimenez-Cano et al., 2013). The use of such systems provides a variety of new applications, ranging from manufacturing to robotic assistance. However, since most mobile platforms are restricted to the ground, the mobility can be compromised if the task requires, for instance, climbing stairs or reaching difficult places to perform the manipulation.

Unmanned aerial vehicles (UAVs), on the other hand, have been used in several applications, such as exploration, detection, localization and monitoring. However, they are mainly considered as platforms for environmental sensing. Many of their tasks are limited since they cannot directly interact with the environment. Therefore, many researchers are working on aerial manipulators, which are analogous to (terrestrial) mobile manipulators, but are composed of a manipulator attached to an aerial platform. The use of aerial manipulators amplifies the range of tasks, such as in the construction of high platforms and load transportation to devastated areas (Korpela et al., 2012, 2014).

Research involving aerial manipulators uses mainly quadrotor or helicopters as aerial platforms (Arleo et al., 2013; Jimenez-Cano et al., 2013; Orsag et al., 2013) and some of the projects use manipulators with a gripper (Danko & Oh, 2014) or even more than one arm (Korpela et al., 2011; Orsag et al., 2013). Danko & Oh (2014) showed that the manipulator design has an important impact on the system performance, and then presented a hyper-redundant manipulator that can perform tasks more efficiently.

Those researches also proposed some models and control strategies to perform aerial manipulation tasks. Arleo et al. (2013) developed a whole-body model of an aerial manipulator and a cascade controller to track the desired end-effector trajectory by considering the inverse kinematics. Similarly, Orsag et al. (2013) presented a whole-body model, but the dynamics model was reduced to two scenarios: i) Manipulation stage, where the manipulator performs a certain task while the quadrotor remains hovering; and ii) Flying stage: the aerial manipulator flies to a desired position, while the manipulator remains still in a home configuration.

Heredia & Jimenez-Cano (2014) designed an aerial manipulator to perform outdoor tasks and used a backstepping control law. Korpela et al. (2013) developed two models for their system, having a UAV model and a manipulator model. However, the controllers considered the influence of the end-effector movement on the center of mass of the UAV.

The present paper models the whole-body dynamics of an aerial manipulator, considering a quadrotor UAV coupled to a three-link planar manipulator. The control strategy is composed of two controllers in a cascade scheme. In the inner loop control, an inverse dynamics controller is designed in the configuration space to track the trajectory generated by the outer loop. In the latter, the kinematic controller performs the path tracking of the end-effector. To evaluate the proposed control strategy, two simulations that consider one scenario without disturbances and other with disturbances are carried out.

The paper is organized as follows: Section 2 presents the mathematical background related to dual quaternions and kinematic modeling, whereas Sections 3 and 4 present the main contributions of the paper, that is, the system modeling and control design. Section 5 reports the simulations results to certify the approach and finally, Section 6 concludes the paper.

2 Mathematical Background

The use of dual quaternion algebra in robotics research has been increasing in recent years, thanks to its computational efficiency, absence of representational singularities and modeling expressiveness—for instance, dual quaternions are used to represent rigid motions, twists, wrenches, and geometrical primitives (Adorno, 2011). This section briefly describes the dual quaternion algebra and its use in robot kinematic modeling.

2.1 Dual quaternion algebra

Quaternions, denoted by the set $\mathbb{H}$, are an extension of complex numbers and are defined as $\boldsymbol{h} \triangleq h_1 + \hat{\imath} h_2 + \hat{\jmath} h_3 + \hat{k} h_4$, where $h_1, h_2, h_3, h_4 \in \mathbb{R}$ and $\hat{\imath}^2 = \hat{\jmath}^2 = \hat{k}^2 = \hat{\imath}\hat{\jmath}\hat{k} = -1$. Dual quaternions, denoted by the set $\mathcal{H}$, are composed of two quaternions in addition to the dual unit ε, which has the properties $\varepsilon \neq 0$ and $\varepsilon^2 = 0$ (Selig, 2005). More specifically, a dual quaternion is given by $\underline{\boldsymbol{x}} \triangleq h_1 + \hat{\imath} h_2 + \hat{\jmath} h_3 + \hat{k} h_4 + \varepsilon \left(h_5 + \hat{\imath} h_6 + \hat{\jmath} h_7 + \hat{k} h_8 \right)$ and we refer to $\mathcal{P}(\underline{\boldsymbol{x}}) \triangleq h_1 + \hat{\imath} h_2 + \hat{\jmath} h_3 + \hat{k} h_4$ and $\mathcal{D}(\underline{\boldsymbol{x}}) \triangleq h_5 + \hat{\imath} h_6 + \hat{\jmath} h_7 + \hat{k} h_8$ as the primary part and dual part of $\underline{\boldsymbol{x}}$, respectively. Sometimes, it is convenient to map dual quaternions into an eight-dimensional vector, by means of the mapping $\operatorname{vec} : \mathcal{H} \to \mathbb{R}^8$, where $\operatorname{vec} \underline{\boldsymbol{x}} \triangleq \begin{bmatrix} h_1 & \cdots & h_8 \end{bmatrix}^T$.

Although quaternions are commonly used to represent rigid body rotations in three-dimensional space, they are also used to represent translations (Selig, 2005). For instance, given the position $\begin{bmatrix} p_x & p_y & p_z \end{bmatrix}^T$, the corresponding quaternion is represented by $\boldsymbol{p} = \hat{\imath} p_x + \hat{\jmath} p_y + \hat{k} p_z$. On the other hand, the orientation is represented by $\boldsymbol{r} = \cos(\phi/2) + \boldsymbol{n} \sin(\phi/2)$, where ϕ is the rotation angle around axis $\boldsymbol{n} = \hat{\imath} n_x + \hat{\jmath} n_y + \hat{k} n_z$.

Both translation and rotation—i.e., a complete rigid motion—is represented in a unified way by a unit dual quaternion $\underline{\boldsymbol{x}} = \boldsymbol{r} + (1/2)\,\varepsilon \boldsymbol{p}\boldsymbol{r}$. The set of *unit* dual quaternions form the algebraic group $\mathrm{Spin}(3) \ltimes \mathbb{R}^3$.

A sequence of rigid transformations is represented by a sequence of unit dual quaternions multiplications. For example, given that $\underline{\boldsymbol{x}}_1^0$ represents frame $\mathcal{F}_1$ with respect to $\mathcal{F}_0$ and $\underline{\boldsymbol{x}}_2^1$ represents frame $\mathcal{F}_2$ with respect to $\mathcal{F}_1$, then $\mathcal{F}_2$ with respect to $\mathcal{F}_0$ is $\underline{\boldsymbol{x}}_2^0 = \underline{\boldsymbol{x}}_1^0 \underline{\boldsymbol{x}}_2^1$.

Although dual quaternion multiplication is not commutative, Hamilton operators can be used to conveniently switch terms in a dual quaternion multiplication (Adorno, 2011). More specifically, given $\underline{\boldsymbol{x}}_1, \underline{\boldsymbol{x}}_2 \in \mathcal{H}$, the Hamilton operators $\overset{+}{\boldsymbol{H}}(\cdot)$ and $\overset{-}{\boldsymbol{H}}(\cdot)$ are matrices that satisfy $\operatorname{vec}(\underline{\boldsymbol{x}}_1 \underline{\boldsymbol{x}}_2) = \overset{+}{\boldsymbol{H}}(\underline{\boldsymbol{x}}_1) \operatorname{vec} \underline{\boldsymbol{x}}_2 = \overset{-}{\boldsymbol{H}}(\underline{\boldsymbol{x}}_2) \operatorname{vec} \underline{\boldsymbol{x}}_1$.

2.2 Kinematics Modeling

The forward kinematics model (FKM) provides the mapping $\underline{\boldsymbol{f}} : \mathbb{R}^n \to \mathrm{Spin}(3) \ltimes \mathbb{R}^3$ between the joint configurations and the end-effector pose; that is, $\underline{\boldsymbol{x}} = \underline{\boldsymbol{f}}(\boldsymbol{q})$, where $\underline{\boldsymbol{x}}$ is the end-effector pose and $\boldsymbol{q}$ is the vector of joint variables. The differential forward kinematics model (DFKM), on the other hand, provides a mapping between the derivatives of the vector of joint variables and the derivatives of the dual quaternion representing the end-effector pose (Adorno, 2011); that is,

$$\operatorname{vec} \dot{\underline{\boldsymbol{x}}} = J \dot{\boldsymbol{q}}, \qquad \operatorname{vec} \ddot{\underline{\boldsymbol{x}}} = \dot{J} \dot{\boldsymbol{q}} + J \ddot{\boldsymbol{q}}, \tag{1}$$

where $J = \partial \operatorname{vec} \underline{\boldsymbol{x}} / \partial \boldsymbol{q}$ is the analytical Jacobian.

3 System Modeling

The structure of the aerial manipulator proposed in this paper consists of a quadrotor coupled to a three-link manipulator. The coordinate systems are the inertial reference frame $\mathcal{F}_0$, the vehicle frame $\mathcal{F}_q$, and the manipulator frame $\mathcal{F}_m$ (Figure 1).

The quadrotor has six degrees of freedom $\boldsymbol{q}_q \triangleq \begin{bmatrix} x & y & z & \phi & \theta & \psi \end{bmatrix}^T$. The variables x, y, and z express the position of $\mathcal{F}_q$ in relation to $\mathcal{F}_0$ and ϕ, θ, and ψ represent the rotations about the moving axes X, Y, and Z, respectively. The manipulator consists of three links connected by revolution joints, which are given by $\boldsymbol{q}_m \triangleq \begin{bmatrix} \beta_1 & \beta_2 & \beta_3 \end{bmatrix}^T$. The whole system has nine degrees of freedom, which are $\boldsymbol{q} \triangleq \begin{bmatrix} \boldsymbol{q}_q^T & \boldsymbol{q}_m^T \end{bmatrix}^T$.

Next, the kinematics and dynamics modeling of the system are developed, so that the aerial manipulator are able to perform tasks defined at the end-effector level.

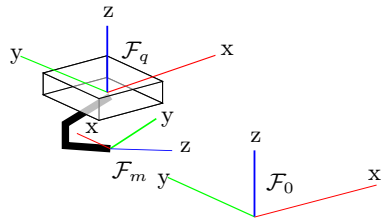

Figure 1: Coordinate systems: $\mathcal{F}_0$ is the inertial reference frame; $\mathcal{F}_q$ is the vehicle frame; and $\mathcal{F}_m$ is the manipulator frame.

Table 1: DH parameters of the manipulator

Link	d (m)	θ (rad)	a (m)	α (rad)
L_1	0	$\pi/4+\beta_1$	0.15	0
L_2	0	$\pi/4+\beta_2$	0.15	0
L_3	0	$\pi/4+\beta_3$	0.15	$\pi/2$

3.1 Kinematic Modeling

The FKM of the aerial manipulator takes into account quadrotor and manipulator models to represent the pose of the end-effector, represented by the coordinate system $\mathcal{F}_m$, with respect to the inertial frame $\mathcal{F}_0$. The quadrotor FKM is given by $\underline{\boldsymbol{x}}_q=\boldsymbol{r}_q+(1/2)\,\varepsilon\boldsymbol{p}_q\boldsymbol{r}_q$, where $\boldsymbol{r}_q=\boldsymbol{r}_z\boldsymbol{r}_y\boldsymbol{r}_x$ and $\boldsymbol{p}_q=\hat{\imath}x+\hat{\jmath}y+\hat{k}z$, being $\boldsymbol{r}_x$ a rotation ϕ around the moving axis X, $\boldsymbol{r}_y$ a rotation θ around the moving axis Y, and $\boldsymbol{r}_z$ a rotation ψ around the moving axis Z.

The manipulator FKM is obtained by using the standard Denavit-Hartenberg (DH) convention—whose parameters are shown in Table 1—applied to dual quaternion algebra (Adorno, 2011). Furthermore, an additional rotation in the end-effector frame is considered, so that the z-axis is the approach direction, the y-axis is the sliding direction (the direction along which the gripper slides to open and close), and the x-axis is the normal direction of the plane formed by preceding axes (Spong et al., 2006). This rotation is represented by $\underline{\boldsymbol{x}}_E^{L_3}=(\cos(\pi/4)+\sin(\pi/4)\,\hat{\imath})$. The manipulator FKM is thus given by $\underline{\boldsymbol{x}}_m=\underline{\boldsymbol{x}}_{L_1}\underline{\boldsymbol{x}}_{L_2}\underline{\boldsymbol{x}}_{L_3}\underline{\boldsymbol{x}}_E^{L_3}$.

The FKM of the whole system $\underline{\boldsymbol{x}}$ is

$$\underline{\boldsymbol{x}}=\underline{\boldsymbol{x}}_q\underline{\boldsymbol{x}}_a\underline{\boldsymbol{x}}_m, \tag{2}$$

where $\underline{\boldsymbol{x}}_a=\boldsymbol{r}_a+(1/2)\,\varepsilon\boldsymbol{p}_a\boldsymbol{r}_a$ is a transformation from $\mathcal{F}_q$ to the manipulator basis and $\boldsymbol{r}_a=(\cos(\pi/4)-\sin(\pi/4)\,\hat{\imath})\left(\cos(\pi/2)-\sin(\pi/2)\,\hat{k}\right)$ and $\boldsymbol{p}_a=-0.075\hat{k}$.

In order to obtain the DFKM of the whole system, we perform the time derivative of (2) and map the resulting equation to $\mathbb{R}^8$, which yields

$$\operatorname{vec}\dot{\underline{\boldsymbol{x}}}=J\dot{\boldsymbol{q}}, \tag{3}$$

where $J\triangleq\left[\bar{\boldsymbol{H}}\left(\underline{\boldsymbol{x}}_a\underline{\boldsymbol{x}}_m\right)J_q \quad \overset{+}{\boldsymbol{H}}\left(\underline{\boldsymbol{x}}_q\underline{\boldsymbol{x}}_a\right)J_m\right]$.

3.2 Dynamic Modeling

The dynamic equations are used in the inverse dynamics controller design, as well as in the system representation for simulation purposes. They are obtained through Euler-Lagrange formulation (Spong et al., 2006) and are described by

$$M(\boldsymbol{q})\,\ddot{\boldsymbol{q}}+C(\boldsymbol{q},\dot{\boldsymbol{q}})\,\dot{\boldsymbol{q}}+G(\boldsymbol{q})=B(\boldsymbol{q})\,\boldsymbol{\Gamma}, \tag{4}$$

where $M(\boldsymbol{q})$ is the inertia matrix, $C(\boldsymbol{q},\dot{\boldsymbol{q}})$ is the Coriolis matrix, $G(\boldsymbol{q})$ the gravitational forces vector, $B(\boldsymbol{q})$ is the coupling matrix, and $\boldsymbol{\Gamma}=[\ f_1\ \ f_2\ \ f_3\ \ f_4\ \ \tau_1\ \ \tau_2\ \ \tau_3\ ]^T$ are the applied forces and torques. More specifically, f_i, with $i=\{1,\ldots,4\}$, is the thrust generated by the i-th rotor (Mistler et al., 2001; Raffo, 2011), and τ_j, with $j=\{1,2,3\}$, is the torque at the j-th manipulator joint.

Our aerial manipulator is an underactuated system, since it has less actuators than degrees of freedom (Raffo, 2011). Indeed, angles ϕ and θ (which correspond to roll and pitch, respectively) can only be stabilized, which means that it is not possible to regulate them into a specific operation point at the same time instant in which the others DOF are regulated.

The coupling matrix $B(\boldsymbol{q})$ is given by

$$B(\boldsymbol{q})=\begin{bmatrix}N(\boldsymbol{q}) & 0_{4\times3}\\ 0_{3\times3} & I_3\end{bmatrix},$$

where

$$N(\boldsymbol{q})=\begin{bmatrix}W^T & 0_{3\times3}\\ 0_{3\times3} & R\end{bmatrix}\begin{bmatrix}N_1 & N_2\\ N_3 & N_4\end{bmatrix},\ \text{with}$$

$$N_1=\begin{bmatrix}0 & lc_{\alpha_T}\\ -lc_{\alpha_T} & 0\\ \frac{k_t c_{\alpha_T}}{b} & -\frac{k_t c_{\alpha_T}}{b}\end{bmatrix},\quad N_2=\begin{bmatrix}0 & -lc_{\alpha_T}\\ lc_{\alpha_T} & 0\\ \frac{k_t c_{\alpha_T}}{b} & -\frac{k_t c_{\alpha_T}}{b}\end{bmatrix},$$

$$N_3=\begin{bmatrix}-s_{\alpha_T} & 0\\ 0 & -s_{\alpha_T}\\ c_{\alpha_T} & c_{\alpha_T}\end{bmatrix},\quad N_4=\begin{bmatrix}s_{\alpha_T} & 0\\ 0 & s_{\alpha_T}\\ c_{\alpha_T} & c_{\alpha_T}\end{bmatrix},$$

and $c_{\alpha_T}\triangleq\cos\alpha_T$, $s_{\alpha_T}\triangleq\sin\alpha_T$. Furthermore, R is the rotation matrix that describes the orientation of the body frame $\mathcal{F}_q$ with respect to the inertial frame $\mathcal{F}_0$; the matrix W relates the angular velocity of the body frame to the time derivative of the Euler angles (Raffo, 2011); $I_n\in\mathbb{R}^{n\times n}$ is the identity matrix and $0_{n\times m}\in\mathbb{R}^{n\times m}$ is the zero matrix; $l=0.332$m is the distance between the center of mass and the rotor; $b=9.5\cdot10^{-6}\,\mathrm{N}\cdot\mathrm{s}^2$ is the rotor's thrust coefficient; $k_t=1.7\cdot10^{-7}\,\mathrm{N}\cdot\mathrm{m}\cdot\mathrm{s}^2$ is the rotor's drag coefficient; and $\alpha_T=5^{\mathrm{o}}$ is the angle of the rotors with respect to the vertical axis. Thanks to this angle, the thrust forces also generate longitudinal and lateral movements on axis X and axis Y, respectively.

The model parameters of the aerial manipulator are shown in Table 2, where the first link corresponds to the quadrotor and the other links correspond to the manipulator ones.

Table 2: Model parameters of the aerial vehicle.

Link	m_i (kg)	I_{xx} $(kg.m^2)$	I_{yy} $(kg.m^2)$	I_{zz} $(kg.m^2)$
1	2.24	0.0363	0.0363	0.0615
2	0.2	$7.53\,10^{-6}$	$6.48\,10^{-6}$	$6.48\,10^{-6}$
3	0.2	$7.53\,10^{-6}$	$6.48\,10^{-6}$	$6.48\,10^{-6}$
4	0.2	$7.53\,10^{-6}$	$6.48\,10^{-6}$	$6.48\,10^{-6}$

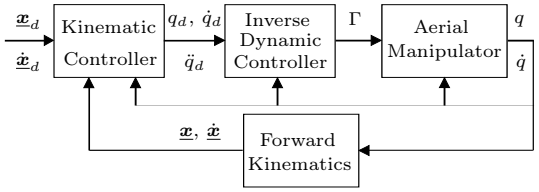

Figure 2: Block diagram of the control architecture.

4 Control Design

The main objective of the control system is to perform tasks at the end-effector level, in which it is required to track both desired pose $\underline{\boldsymbol{x}}_d$ and desired velocities $\dot{\underline{\boldsymbol{x}}}_d$ of the end-effector, while keeping the whole system stable.

The cascade control structure is composed of two levels. In the outer loop, the kinematic controller $\boldsymbol{v}_c$ computes the joint-space motion references $\boldsymbol{q}_d$, $\dot{\boldsymbol{q}}_d$, and $\ddot{\boldsymbol{q}}_d$, which are tracked by an inverse dynamics controller $\boldsymbol{\Gamma}$ in the inner loop. This scheme is summarized in Figure 2.

In order to stabilize variables ϕ and θ, while performing the task in the end-effector level, the kinematic control law v_c is divided into two parts:

$$\boldsymbol{v}_c = \begin{bmatrix}\boldsymbol{v}_1^T & \boldsymbol{v}_2^T\end{bmatrix}^T. \quad (5)$$

Therefore, we also split the Jacobian matrix into two blocks—J_1 and J_2—where J_1, which is related to ϕ and θ, is composed of the first two columns of $J(\boldsymbol{q})$, and J_2 is composed of the remaining columns. The vector $\boldsymbol{q}$ of generalized coordinates is also partitioned accordingly, that is, $\boldsymbol{q}^T = \begin{bmatrix}\boldsymbol{q}_1^T & \boldsymbol{q}_2^T\end{bmatrix}^T$.

The first part of the controller, $\boldsymbol{v}_1 = K_{p2}\begin{bmatrix}\dot{\phi} & \dot{\theta}\end{bmatrix}^T \in \mathbb{R}^2$, is a proportional controller of the variables $\dot{\phi}$ and $\dot{\theta}$, with gain matrix $K_{p2} \in \mathbb{R}^{2\times 2}$. The desired values for these velocities are zero, since the goal is to maintain the quadrotor stable while performing the task. The second part, $\boldsymbol{v}_2 \in \mathbb{R}^7$, is based on the DFKM, with an additional control law $\boldsymbol{U}$ in the null space of matrix J_2, and its objective is to track the trajectory, while keeping the joints of the manipulator as far as possible from their limits. Thus, $\boldsymbol{v}_2$ is given by

$$\boldsymbol{v}_2 = J_2^{\#}\left(\boldsymbol{Q}_x - \dot{J}_2\dot{\boldsymbol{q}}_2\right) + \left(I_7 - J_2^{\#}J_2\right)\boldsymbol{U}, \quad (6)$$

where $\boldsymbol{Q}_x \triangleq K_{pc}\,\mathrm{vec}\,(\underline{\boldsymbol{x}}_d - \underline{\boldsymbol{x}}) + K_{dc}\,\mathrm{vec}\,(\dot{\underline{\boldsymbol{x}}}_d - \dot{\underline{\boldsymbol{x}}})$, and $K_{pc} \in \mathbb{R}^{8\times 8}$ and $K_{dc} \in \mathbb{R}^{8\times 8}$ are proportional and derivative gains matrices, respectively. Considering $d(\boldsymbol{q}_m) \triangleq \sum_{i=1}^{3}\bar{d}_i$, where $\bar{d}_i \triangleq 1/2\beta_i^2$, with $i=\{1,2,3\}$ and $\boldsymbol{d}_p \triangleq \partial d(\boldsymbol{q}_m)/\partial \boldsymbol{q}_m$, the secondary control law is $\boldsymbol{U} \triangleq J_{ns}^{\#}\left(K_{ns1}d(\boldsymbol{q}_m) + K_{ns2}\dot{d}(\boldsymbol{q}_m) - \dot{\boldsymbol{d}}_p\dot{\boldsymbol{q}}_m\right)$, where $J_{ns} = \begin{bmatrix}0_{1\times 4} & \boldsymbol{d}_p\end{bmatrix}$, and $K_{ns1} \in \mathbb{R}$ and $K_{ns2} \in \mathbb{R}$ are proportional and derivative scalar gains, respectively.

The inverse dynamic controller is given by

$$\boldsymbol{\Gamma} = B(\boldsymbol{q})^{\#}\left(M(\boldsymbol{q})\,\boldsymbol{v} + C(\boldsymbol{q},\dot{\boldsymbol{q}})\,\dot{\boldsymbol{q}} - G(\boldsymbol{q})\right), \quad (7)$$

where $\boldsymbol{v} \triangleq K_p(\boldsymbol{q}_d - \boldsymbol{q}) + K_d(\dot{\boldsymbol{q}}_d - \dot{\boldsymbol{q}}) + \ddot{\boldsymbol{q}}_d$ is a PD controller with feedforward action in acceleration and $K_p \in \mathbb{R}^{9\times 9}$ and $K_d \in \mathbb{R}^{9\times 9}$ are diagonal matrices representing the proportional and derivative gains, and $\ddot{\boldsymbol{q}}_d \triangleq \boldsymbol{v}_c$. The values of $\dot{\boldsymbol{q}}_d$ and $\boldsymbol{q}_d$ are obtained by integration of $\ddot{\boldsymbol{q}}_d$.

5 Results and discussions

The proposed control strategy has been tested via numerical simulations in Matlab/Simulink environment. We have considered the quadrotor model described by Raffo (2011) and the manipulator parameters were obtained through the designed CAD model. The gain matrices K_{pc}=blkdiag$(0.0045\,I_4; 0.006\,I_4)$ and K_{dc}=blkdiag$(0.04\,I_4; 0.078\,I_4)$ in (6) are adjusted empirically. The submatrices related to the primary parts of the pose and pose derivative errors have lower values than the submatrices related to their dual parts (which embed the translational components), because the system's translational dynamics is slower than its rotational dynamics. The inverse dynamic controller's gain matrix K_p=blkdiag$(0_{2\times 2}; I_4; 2\,I_3)$ is adjusted taking into account that ϕ and θ cannot be controlled, and therefore their gains are zero. On the other hand, the gain matrix K_d=blkdiag$(50\,I_2; I_4; 50\,I_3)$ is adjusted considering that ϕ, θ and β_i, with $i=\{1,2,3\}$, must stabilize faster than the other variables. The same arguments have been used to adjust $K_{p2} = -5\,I_2$, K_{ns1}=0.5, and K_{ns2}=100.

An external disturbance vector $\bar{\boldsymbol{\Gamma}} = \begin{bmatrix}0_{1\times 3} & 0.1 & 0_{1\times 3}\end{bmatrix}^T$ is also applied to the system at t=400 s. The end-effector task consists in following a circular trajectory defined as

$$\underline{\boldsymbol{x}}_d = \left(1 + \varepsilon\left(C_1\hat{\imath} + C_2\hat{\jmath} + (3 - 4C_1)\,\hat{k}\right)\right)\underline{\boldsymbol{x}}(0), \quad (8)$$

along with $\dot{\underline{\boldsymbol{x}}}_d$, which is directly computed taking the time derivative of (8). In addition, $C_1 \triangleq (1/2)\cos(wt)$, and $C_2 \triangleq (1/2)\sin(wt)$, where $w = 2\pi/T_s$ is the angular velocity and $T_s = 1000$ s is the total simulation time.

Figures 3–7 show the simulations results of the path tracking for the aerial manipulator, considering one scenario without disturbances and other with disturbances. In detail, Figure 3 shows

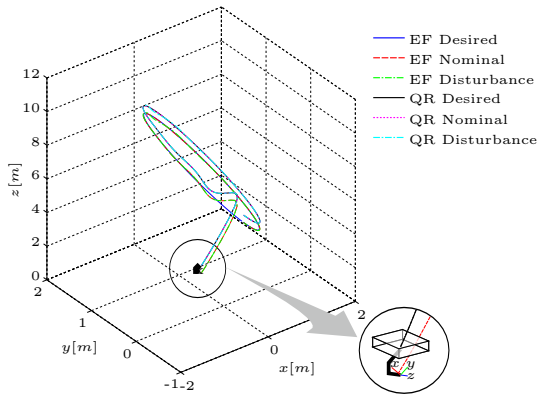

Figure 3: Desired and actual trajectories for the end-effector (EF) and the quadrotor (QR).

a 3D view of the trajectory followed by end-effector and quadrotor. Even in the presence of disturbances, the aerial manipulator followed the specified trajectory while remaining stable. The time response of each component of the dual quaternion is shown in Figure 4. Despite the disturbance, each component converges asymptotically to its desired reference.

Figure 5a presents the time response of the Euler angles corresponding to the quadrotor orientation. Since the desired orientation is always constant—see (8)—we conclude that the cascade scheme had a satisfactory performance as the variations in each orientation component were very small and fluctuated around 0 rad, which ensures stability. Figure 5b presents the time evolution of the quadrotor's translational motions, indicating that the control strategy was capable of guiding the vehicle smoothly. Moreover, the controllers provided null steady-state error in both translational and rotational motions. Figure 6 shows the time response of the manipulator joint angles. As one can see, the secondary control objective, which was projected in the null space of the primary task, was successful in keeping these angles close to their desired values, which correspond to the manipulator home configuration ($\pi/4$ for all angles). The error in these angles were non-zero, as expected, due to the requirements imposed by the primary task to follow the desired trajectory. Finally, Figure 7 shows the control efforts. More specifically, the upper graph shows the thrust of each rotor of the vehicle, whereas the lower graph shows the torques in each joint of the manipulator. Both indicate that the inputs were not aggressive, even in the presence of disturbances.

It is also possible to note the effects of the whole-body control in the results. For example, due to the geometric restrictions of the planar manipulator, the end-effector can move only along axes X and Z. In the beginning of the simulation, the end-effector is located below the desired position specified by the trajectory. Since at the beginning of the simulation the first two manipulator

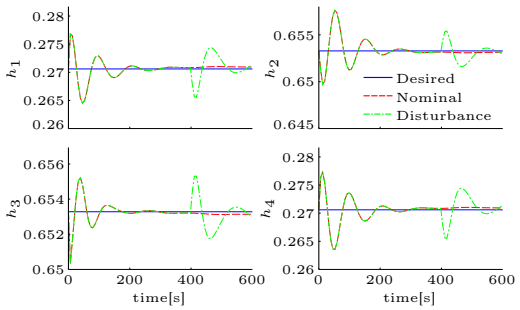

(a) Primary part of $\underline{\boldsymbol{x}}$.

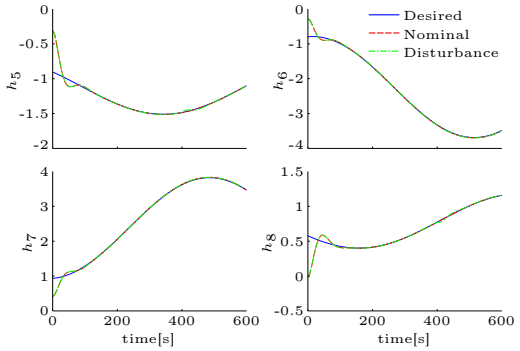

(b) Dual part of $\underline{\boldsymbol{x}}$.

Figure 4: Desired and actual trajectories of $\underline{\boldsymbol{x}}$.

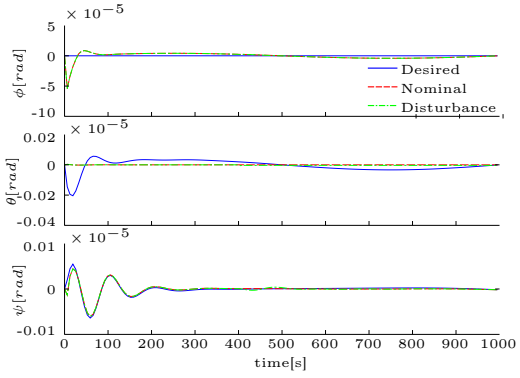

(a) Orientation.

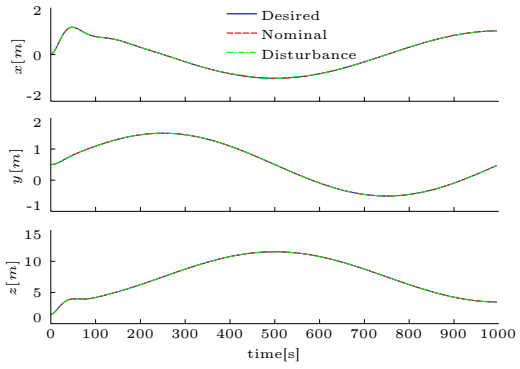

(b) Position.

Figure 5: Variables of the quadrotor during the tracking of the circular trajectory.

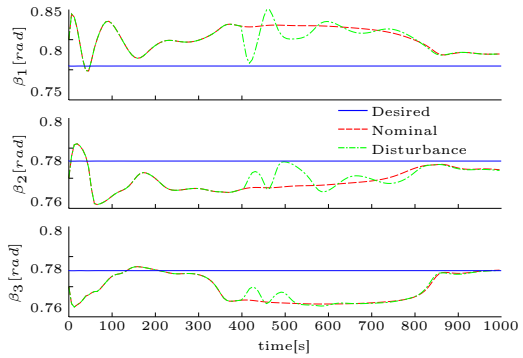

Figure 6: Time evolution of the joint angles of the 3 DOF manipulator arm for the circular trajectory.

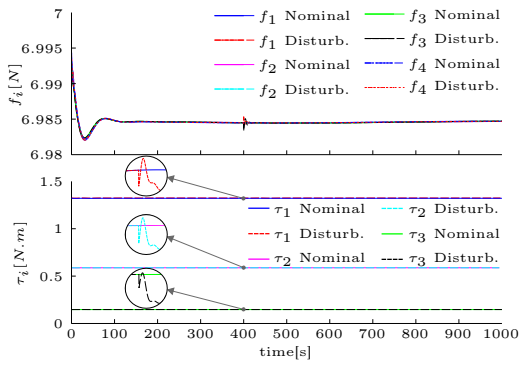

Figure 7: Time evolution of the control efforts.

links move in such a way that the displacement in Z is reduced (when it should be increased), the third link and the quadrotor move in the opposite direction in order to compensate for the motion of these first two links, as shown in Figure 5b and Figure 6 between 0s and 100s.

6 Conclusions

Aerial robotics is evolving to include not only systems with sensing capabilities but also with the possibility to act on the environment, and particularly with manipulation capabilities. This paper has proposed a new kinematic model, based on dual quaternion algebra, for an unmanned aerial vehicle serially coupled to a manipulator robot. In addition, a cascade control strategy, which comprises a kinematic controller and an inverse dynamics controller, has been proposed to track a desired trajectory for the end-effector while keeping the system stable and avoiding the manipulator joint limits. Finally, the performance of the proposed control strategy has been evaluated through simulation results, showing that a trajectory defined for the manipulator end-effector is successfully tracked while the quadrotor remains stable.

Acknowledgments

This work has been supported by the Brazilian agencies CAPES, CNPq and FAPEMIG.

References

Adorno, B. V. (2011). *Two-arm manipulation: from manipulators to enhanced human-robot collaboration.* PhD thesis, Université Montpellier 2.

Arleo, G., Caccavale, F., Muscio, G., & Pierri, F. (2013). Control of quadrotor aerial vehicles equipped with a robotic arm. In *21st Mediterranean Conf. on Control and Automation* (pp. 1174–1180).

Danko, T. W. & Oh, P. Y. (2014). Design and control of a hyper-redundant manipulator for mobile manipulating unmanned aerial vehicles. *Journal of Intelligent and Robotic Systems: Theory and Applications*, 73(1-4), 709–723.

Heredia, G. & Jimenez-Cano, A. (2014). Control of a multirotor outdoor aerial manipulator. In *Intl. Conf. on Intelligent Robots and Systems IEEE/RSJ* (pp. 3417 – 3422).

Jimenez-Cano, A. E., Martin, J., Heredia, G., Ollero, A., & Cano, R. (2013). Control of an aerial robot with multi-link arm for assembly tasks. In *IEEE Intl. Conf. on Robotics and Automation* (pp. 4916–4921).

Korpela, C., Orsag, M., & Oh, P. (2014). Towards Valve Turning using a Dual-Arm Aerial Manipulator. In *Intl. Conf. on Unmanned Aircraft Systems* (pp. 3411–3416).

Korpela, C., Orsag, M., Pekala, M., & Oh, P. (2013). Dynamic stability of a mobile manipulating unmanned aerial vehicle. In *IEEE Intl. Conf. on Robotics and Automation* (pp. 4922–4927).

Korpela, C. M., Danko, T. W., & Oh, P. Y. (2011). Designing a system for mobile manipulation from an Unmanned Aerial Vehicle. *IEEE Conf. on Technologies for Practical Robot Applications*, (pp. 109–114).

Korpela, C. M., Danko, T. W., & Oh, P. Y. (2012). MM-UAV: Mobile manipulating unmanned aerial vehicle. *Journal of Intelligent and Robotic Systems: Theory and Applications*, 65(1-4), 93–101.

Mistler, V., Benallegue, A., & M'Sirdi, N. (2001). Exact linearization and noninteracting control of a 4 rotors helicopter via dynamic feedback. In *IEEE Intl. Conf. on Robotics and Automation* (pp. 586–593).

Orsag, M., Korpela, C., & Oh, P. (2013). Modeling and control of MM-UAV: Mobile manipulating unmanned aerial vehicle. *Journal of Intelligent and Robotic Systems: Theory and Applications*, 69(1-4), 227–240.

Raffo, G. (2011). *Robust Control Strategies for a QuadRotor Helicopter an Underactuated Mechanical System.* PhD thesis, Universidad de Sevilla.

Selig, J. M. (2005). *Geometric fundamentals of robotics.* Springer-Verlag New York Inc., 2nd edition.

Spong, M., Hutchinson, S., & Vidyasagar, M. (2006). *Robot Modeling and Control.* USA, 6 ed. edition.